Analysis of granular flow in a pebble-bed nuclear reactor

Chris H. Rycroft,[1] Gary S. Grest,[2] James W. Landry,[3] and Martin Z. Bazant[1]
[1]*Department of Mathematics, Massachusetts Institute of Technology, Cambridge, Massachusetts 02139, USA*
[2]*Sandia National Laboratories, Albuquerque, New Mexico 87185, USA*
[3]*Lincoln Laboratory, Massachusetts Institute of Technology, Lexington, Massachusetts 02420, USA*
(Received 15 February 2006; published 24 August 2006)

Pebble-bed nuclear reactor technology, which is currently being revived around the world, raises fundamental questions about dense granular flow in silos. A typical reactor core is composed of graphite fuel pebbles, which drain very slowly in a continuous refueling process. Pebble flow is poorly understood and not easily accessible to experiments, and yet it has a major impact on reactor physics. To address this problem, we perform full-scale, discrete-element simulations in realistic geometries, with up to 440 000 frictional, viscoelastic 6-cm-diam spheres draining in a cylindrical vessel of diameter 3.5 m and height 10 m with bottom funnels angled at 30° or 60°. We also simulate a bidisperse core with a dynamic central column of smaller graphite moderator pebbles and show that little mixing occurs down to a 1:2 diameter ratio. We analyze the mean velocity, diffusion and mixing, local ordering and porosity (from Voronoi volumes), the residence-time distribution, and the effects of wall friction and discuss implications for reactor design and the basic physics of granular flow.

DOI: 10.1103/PhysRevE.74.021306 PACS number(s): 45.70.Mg

I. INTRODUCTION

A. Background

A worldwide effort is underway to develop more economical, efficient, proliferation resistant, and safer nuclear power [1]. A promising generation IV reactor design is the uranium-based, graphite-moderated, helium-cooled very-high-temperature reactor [2], which offers meltdown-proof passive safety, convenient long-term waste storage, modular construction, and a means of nuclear-assisted hydrogen production and desalination. In one embodiment, uranium dioxide is contained in microspheres dispersed in spherical graphite pebbles, the size of billiard balls, which are very slowly cycled through the core in a dense granular flow [3,4]. Control rods are inserted in graphite bricks of the core vessel, so there are no obstacles to pebble flow.

The pebble-bed reactor (PBR) concept, which originated in Germany in the 1950s, is being revisited by several countries, notably China [5] (HTR-10 [6]) and South Africa [3] (PBMR [7]), which plan large-scale deployment. In the United States, the Modular Pebble Bed Reactor (MPBR) [4,8] is a candidate for the next generation nuclear plant of the Department of Energy. A notable feature of MPBR (also present in the original South African design) is the introduction of graphite moderator pebbles, identical to the fuel pebbles but without the uranium microspheres. The moderator pebbles form a dynamic central column, which serves to flatten the neutron flux across the annular fuel region without placing any fixed structures inside the core vessel. The annular fuel region increases the power output and efficiency, while preserving passive safety. In the bidisperse MPBR, the moderator pebbles are smaller to reduce the permeability of the central column and thus focus helium gas on the outer fuel annulus. The continuous refueling process is a major advantage of pebble-bed reactors over other core designs, which typically require shutting down for a costly dismantling and reconstruction. The random cycling of pebbles through a flowing core also greatly improves the uniformity of fuel burnup.

In spite of these advantages, however, the dynamic core of a PBR is also a cause for concern among designers and regulators, since the basic physics of dense granular flow is not fully understood. Indeed, no reliable continuum model is available to predict the mean velocity in silos of different shapes [9], although the empirical kinematic model [10–12] provides a reasonable fit near the orifice in a wide silo [13–16]. A microscopic model for random-packing dynamics has also been proposed [17] and fitted to reproduce drainage in a wide silo [18], but a complete statistical theory of dense granular flow is still lacking. The classical kinetic theory of gases has been successfully applied to dilute granular flows [19–21], in spite of problems with inelastic collisions [22], but it clearly breaks down in dense flows with long-lasting, frictional contacts [16,23], as in pebble-bed reactors. Plasticity theories from soil mechanics might seem more appropriate [12], but they cannot describe flows in silos of arbitrary shape and often lead to violent instabilities [24,25], although a stochastic flow rule [26] may resolve these difficulties and eventually lead to a general theory.

For now, experiments provide important, although limited, information about dense granular flows. Many experiments have been done on drainage flows in quasi-two-dimensional (quasi-2D) silos where particles are tracked accurately at a transparent wall [9,14–16,27]. Some three-dimensional particle tracking in granular materials and colloids has also been done with magnetic resonance imaging [28], confocal microscopy [29], index matching with an interstitial fluid [30], and diffusing-wave spectroscopy [31], although these systems are quite different from a pebble-bed reactor core. Experimental studies of more realistic geometries for PBR have mostly focused on the porosity distribution of static packings of spheres [32,33], which affects helium gas flow through the core [34–36].

As a first attempt to observe pebble dynamics experimentally in a reactor model, the slow flow of plastic beads has

recently been studied in 1:10 scale models of MPBR in two different ways [37]: The trajectories of colored pebbles were recorded (by hand) along a Plexiglas wall in a half-core model, and a single radioactive tracer pebble in the bulk was tracked in three dimensions in a full-core model. Very slow flow was achieved using a screw mechanism at the orifice to approximate the mean exit rate of one pebble per minute in MPBR. These experiments demonstrate the feasibility of the dynamic central column and confirm that pebbles diffuse less than one diameter away from streamlines of the mean flow. However, it is important to gain a more detailed understanding of pebble flow in the entire core to reliably predict reactor power output, fuel efficiency, power peaking, accident scenarios using existing nuclear engineering codes [38,39].

B. Discrete-element simulations

Simulations are ideally suited to provide complete, three-dimensional information in a granular flow. Some simulations of the static random packing of fuel pebbles in a PBR core have been reported [40,41], but in the last few years, large-scale, parallel computing technology has advanced to the stage where it is now possible to carry out simulations of continuous pebble flow in a full-sized reactor geometry using the discrete element method (DEM). In such simulations, each particle is accurately modeled as a sphere undergoing realistic frictional interactions with other particles [42,43]. In this paper, we present DEM simulations which address various outstanding issues in reactor design, such as the sharpness of the interface between fuel and moderator pebbles (in both monodisperse and bidisperse cores), the horizontal diffusion of the pebbles, the geometry dependence of the mean streamlines, the porosity distribution, wall effects, and the distribution of "residence times" for pebbles starting at a given height before exiting the core.

Our simulations are based on the MPBR geometry [4,8], consisting of spherical pebbles with diameter $d=6$ cm in a cylindrical container approximately 10 m high and 3.5 m across. In this design there is a central column of moderating reflector pebbles, surrounded by an annulus of fuel pebbles. The two pebble types are physically identical except that the fuel pebbles contain sand-sized uranium fuel particles. Particles are continuously cycled, so that those exiting the container are reintroduced at the top of the packing. In order to efficiently maintain the central column, a cylindrical guide ring of radius $r_{\text{in}}=14.5d$ extends into the packing to $z=140d$. Reflector pebbles are poured inside, while fuel pebbles are poured outside, and the guide ring ensures that two types do not mix together at the surface. Figure 1 shows the two main geometries that were considered; for much of this analysis, we have concentrated on the case when the exit funnel is sloped at 30°, but since this angle can have a large effect on the pebble flow, we also consider the case of the when the funnel is sloped at 60°. In both cases the radius of the opening at the bottom of the funnel is $r_{\text{exit}}=5d$.

In MPBR, as in most pebble-bed reactors, the drainage process takes place extremely slowly. Pebbles are individually removed from the base of the reactor using a screw mechanism, at a typical rate of one pebble per minute, and

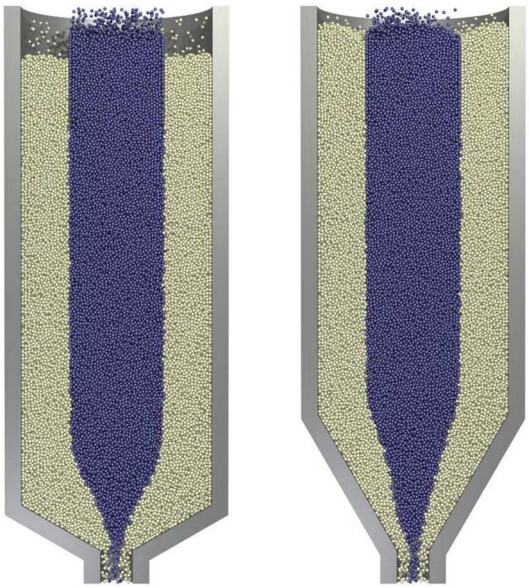

FIG. 1. (Color online) Snapshots of vertical cross sections of the simulations for the two geometries considered in this report. We make use of a cylindrical coordinate system (r,θ,z) where $z=0$ at the orifice. At the base of the container there is a small exit pipe of radius $r_{\text{exit}}=5d$ that extends upwards to $z=10d$. This connects to a conical funnel region, which has slope 30° (left) or 60° (right). The conical wall connects to a cylindrical wall of radius $r_{\text{out}}=29d$, at $z=23.86d$ and $z=51.57d$ for the 30° and 60° reactor geometries, respectively. Particles are poured into the container up to a height of approximately $z=160d$. A cylindrical wall at $r_{\text{in}}=14.5d$ extends down into the packing to a height of $z=140d$ to keep the two types of pebbles mixing at the surface.

the mean residence time of a pebble is 77 days. Carrying out a DEM simulation at this flow rate would make it infeasible to collect enough meaningful data. However, previous experimental work by Choi *et al.* [16] has shown that the regime of slow, dense granular flow is governed by a distinctly nonthermal picture, where particles undergo long-lasting contacts with their neighbors, and the features of the flow are predominately governed by geometry and packing constraints. In particular, they observed that for a large range of hopper drainage experiments, altering the orifice size resulted in a change in the overall flow rate, but did not alter the geometry of the flow profile—the flow velocities were scaled by a constant factor. Furthermore, geometric properties of the flow, such as particle diffusion, were unaffected by the overall flow rate. We therefore chose to study a faster flow regime in which pebbles drain from the reactor exit pipe under gravity. Our results can be related directly to the reactor design by rescaling the time by an appropriate factor.

As well as the two full-scale simulations described above, we also considered a half-size geometry in order to investigate how various alterations in the makeup of the reactor would affect the flow. In particular, we examined a series of bidisperse simulations, in which the diameter of moderator particles in the central column was reduced. As explained in Sec. VIII, this has the effect of reducing the gas permeability of the central column, thus focusing the helium

coolant flow on the hottest region of the reactor core, in and around the fuel annulus. The purpose of the simulations is to test the feasibility of the bidisperse PBR concept, as a function of the size ratio of moderator and fuel pebbles, with regard to the granular flow. It is not clear *a priori* under what conditions the dynamic column will remain stable with little interdiffusion of moderator and graphite pebbles.

To study this issue, we made a sequence of three runs using a half-size reactor geometry. (The smaller core size is needed since the number of smaller pebbles increases as the inverse cube of the diameter ratio.) The geometry is similar to that used above, except that the radius of the cylindrical container is decreased to $15d$, with the guide ring at $r_{\mathrm{in}}=7.5d$. The radius of the exit pipe is decreased to $r_{\mathrm{exit}}=4d$. In the experiments, we keep the diameter of the fuel pebbles fixed at d and use d, $0.8d$, and $0.5d$ for the diameters of the moderator pebbles. The same geometry was also used to study the effect of wall friction by making an additional run with the particle/wall friction coefficient $\mu_w=0$.

The paper is organized as follows. In Sec. II, we discuss the simulation technique that was used and briefly describe its implementation. This is followed with some basic analysis of the velocity profiles and a comparison to the kinematic model in Sec. III. We study diffusion around streamlines in Sec. IV and the distribution of porosity and local ordering in Sec. V. Next, in Sec. VI we examine the residence-time distribution of pebbles in the reactor, which is related to fuel burnup, and in Sec. VII we show that wall friction plays an important role. In Sec. VIII we analyze the bidisperse PBR concept with half-size reactor simulations for a range of pebble-diameter ratios, focusing on the mean flow, diffusion, and mixing. We conclude in Sec. IX by summarizing implications of our study for reactor design and the basic physics of granular flow.

II. MODELS AND METHODS

The DEM simulations are based on a modified version of the model developed by Cundall and Strack [44] to model cohesionless particulates [42,43]. Monodisperse spheres with diameter d interact according to Hertzian, history-dependent contact forces. For a distance $\mathbf{r}$ between a particle and its neighbor, when the particles are in compression, so that $\delta=d-|\mathbf{r}|>0$, then the two particles experience a force $\mathbf{F}=\mathbf{F}_n+\mathbf{F}_t$, where the normal and tangential components are given by

$$\mathbf{F}_n=\sqrt{\delta/d}\left(k_n\delta\mathbf{n}-\frac{\gamma_n\mathbf{v}_n}{2}\right), \tag{1}$$

$$\mathbf{F}_t=\sqrt{\delta/d}\left(-k_t\Delta\mathbf{s}_t-\frac{\gamma_t\mathbf{v}_t}{2}\right). \tag{2}$$

Here, $\mathbf{n}=\mathbf{r}/|\mathbf{r}|$. $\mathbf{v}_n$ and $\mathbf{v}_t$ are the normal and tangential components of the relative surface velocity, and $k_{n,t}$ and $\gamma_{n,t}$ are the elastic and viscoelastic constants, respectively. $\Delta\mathbf{s}_t$ is the elastic tangential displacement between spheres, obtained by integrating tangential relative velocities during elastic deformation for the lifetime of the contact, and is truncated as necessary to satisfy a local Coulomb yield criterion $|\mathbf{F}_t|\le\mu|\mathbf{F}_n|$. Particle-wall interactions are treated identically, though the particle-wall friction coefficient μ_w is set independently.

For the monodispersed system, the spheres have diameter $d=6$ cm, mass $m=210$ g, and interparticle friction coefficient $\mu=0.7$, flowing under the influence of gravity $g=9.81$ ms^{-1}. For the bidispersed systems, the moderator particles have diameter $0.8d$ or $0.5d$. The particle-wall friction coefficient $\mu_w=0.7$ except in one case where we model a frictionless wall, $\mu_w=0.0$. For the current simulations we set $k_t=\frac{2}{7}k_n$ and choose $k_n=2\times10^5\ gm/d$. While this is significantly less than would be realistic for graphite pebbles, where we expect $k_n>10^{10}\ gm/d$, such a spring constant would be prohibitively computationally expensive, as the time step scales as $\delta t\propto k_n^{-1/2}$ for collisions to be modeled effectively. Previous simulations have shown that increasing k_n does not significantly alter physical results [43]. We use a time step of $\delta t=1.0\times10^{-4}\tau$ and damping coefficients $\gamma_n=50\tau^{-1}$ and $\gamma_t=0.0$, where $\tau=\sqrt{d/g}=0.078$ s. All measurements are expressed in terms of d, m, and τ.

The initial configurations are made by extending the inner cylinder from $140d$ to the bottom of the container, adding a wall at the bottom of the container to stop particles from draining and pouring in moderator pebbles into the inner cylinder and fuel pebbles between the inner and outer cylinders until the reactor was loaded. The bottom wall is then removed, the inner cylinder is raised to $140d$, and particles are allowed to drain out of the container. As noted above, particles are recycled with moderator particles reinserted within the inner cylinder and fuel particles between the inner and outer cylinders. All results presented here are after all the particles have cycled through the reactor at least once. The number of moderator and fuel particles was adjusted slightly from the initial filling so that the level at the top of the reactor is approximately equal. For the full-scale simulation with a 30° outlet, the total number of pebbles is 440 000 with 105 011 moderator pebbles and 334 989 fuel pebbles, while for the 60° outlet, the total number of pebbles is 406 405 with 97 463 moderator, and 308 942 fuel pebbles. For the former case, 1×10^6 steps took approximately 13 h on 60 processors on Sandia's Intel Xenon cluster.

For the bidispersed simulations the total number of pebbles is 130 044, 160 423, and 337 715 for the diameter of the moderator particles equal to d, $0.8d$, and $0.5d$, respectively. As the diameter of the moderator pebbles is decreased the number of particles required rapidly increases, since it scales according to the inverse of the diameter cubed.

A snapshot of all the particle positions is recorded every $5\tau=0.39$ s. For the 30° reactor geometry we collected 1087 successive snapshots, totaling 24.9 Gb of data, while for the 60° reactor geometry, we collected 881 successive snapshots, totaling 18.7 Gb of data. A variety of analysis codes written in PERL and C++ were used to sequentially parse the snapshot files to investigate different aspects of the flow. We also created extended data sets, with an additional 440 snapshots for the 30° geometry and 368 snapshots for the 60° geometry, for examining long residence times in Sec. VI.

III. MEAN-VELOCITY PROFILES

A. Simulation results

Since we have a massive amount of precise data about the positions of the pebbles, it is possible to reconstruct the mean flow in the reactor with great accuracy. However, care must be taken when calculating velocity profiles to ensure the highest accuracy. Initial studies of the data showed that crystallization effects near the wall can create features in the velocity profile at a subparticle level, and we therefore chose a method that could resolve this.

By exploiting the axial symmetry of the system, one only needs to find the velocity profile as a function of r and z only. The container is divided into bins, and the mean velocity is determined within each. A particle which is at $\mathbf{x}_n$ at the nth time step and at $\mathbf{x}_{n+1}$ at the $(n+1)$th time step makes a velocity contribution of $(\mathbf{x}_{n+1}-\mathbf{x}_n)/\Delta t$ in the bin which contains its midpoint, $(\mathbf{x}_{n+1}+\mathbf{x}_n)/2$.

In the z direction, we divide the container into strips $1d$ across. However, in the r direction we take an alternative approach. Since the number of pebbles between a radius of r and $r+\Delta r$ is proportional to $r\Delta r$, dividing the container into bins of a fixed width is unsatisfactory, since the amount of data in bins with high r would be disproportionately large. We therefore introduce a new coordinate $s=r^2$. The coordinate s covers the range $0<s<r_{\text{out}}^2$, and we divide the container into regions that are equally spaced in s, of width $1d^2$. The number of pebbles in each bin is therefore roughly equal, allowing for accurate averaging in the bulk and high resolution at the boundary.

This result yields extremely accurate velocity profiles in the cylindrical region of the tank. However, it fails to capture crystallization effects in the conical region: since the particles are aligned with the slope of the walls are averaged over a strip in z of width $1d$, any effects are smeared out across several bins. We therefore scaled the radial coordinate to what it would be if the particle was in the center of the strip. Specifically, if the radius of the container is given by $R(z)$, a particle at (r_n,z_n) is recorded as having radial coordinate $r_nR(z)/R(z_n)$. In the cylindrical region of the tank this has no effect, while in the conical region, it effectively creates trapezoid-shaped bins from which it is easy to see crystallization effects which are aligned with the wall.

The streamlines of the mean flow are shown in Fig. 2 in the two geometries. Streamlines are computed by Lagrangian integration of the DEM velocity field, starting from points at a given height, equally spaced in radius. In each geometry, there is a transition from a nonuniform converging flow in the lower funnel region to a nearly uniform plug flow in the upper cylindrical region, consistent with the standard engineering picture of silo drainage [12]. In the wider funnel, there is a region of much slower flow near the sharp corner at the upper edge of the funnel. Our results for both geometries are quite consistent with particle-tracking data for quasi-2D silos of similar shapes [9] and half-cylinder models of the MPBR core [37], which provide an important validation of our simulations.

We now look more closely at horizontal slices of the velocity field. Figure 3(a) shows several velocity profiles for the 30° case in the narrowing section of the container. As expected, we see a widening of the velocity profile as z increases. We can also see lattice effects, spaced at $\sqrt{3}d$ apart, due to particles crystallizing on the conical wall section.

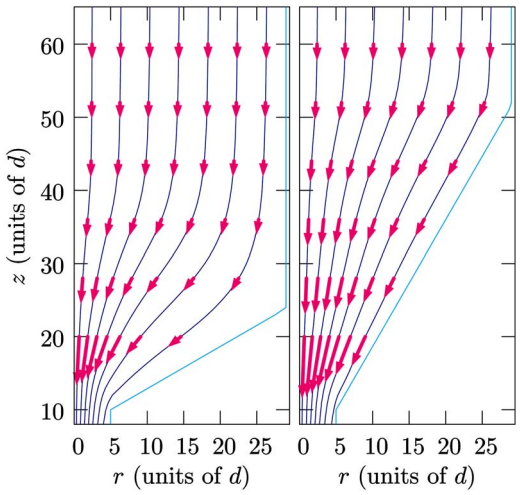

FIG. 2. (Color online) Computed streamlines of the mean flow in the 30° (left) and 60° reactor geometries. Arrows are proportional to the velocity vectors in selected horizontal slices.

Figure 3(b) shows similar plots for several heights in the upper region of the container. At these heights, the velocity profile is roughly uniform across the container. However, a boundary layer of slower velocities, several particle diameters wide, still persists. The average velocities of particles touching the boundary is between one-half and two-thirds that of particles in the bulk; it is expected that this behavior

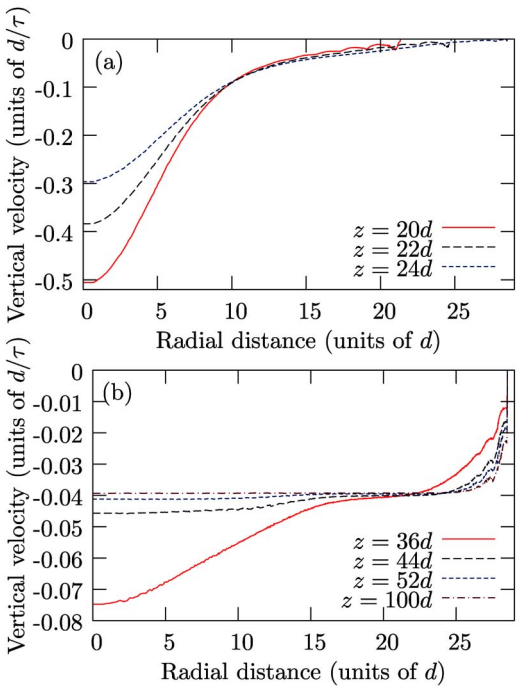

FIG. 3. (Color online) Velocity profiles for the 30° reactor geometry for several low cross sections (a) and several high cross sections (b).

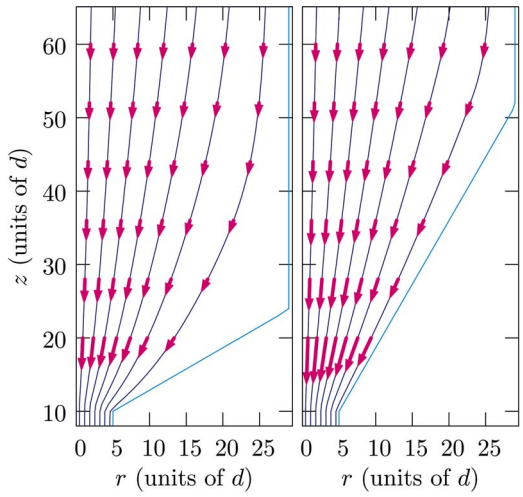

FIG. 4. (Color online) Streamlines of the mean flow in the 30° (left) and 60° reactor geometries for the numerical solution of the kinematic model. Arrows are proportional to the velocity vectors in selected horizontal slices.

is very dependent on particle-wall friction; this issue is studied in more detail in Sec. VII.

High in the container, results for the 60° geometry are very similar to the 30° case (and thus are not shown). However, as would be expected, a significantly different crossover from parabolic flow to pluglike flow in the lower part of the tank is observed, as shown in Fig. 5.

B. Comparison with the kinematic model

Perhaps the only continuum theory available for the mean flow profile in a slowly draining silo is the kinematic model [10–12,45], which postulates that horizontal velocity vector $\mathbf{u}$ is proportional to the horizontal gradient $\boldsymbol{\nabla}_\perp$ of the downward velocity component v (i.e., the local shear rate),

$$\mathbf{u} = b\boldsymbol{\nabla}_\perp v, \tag{3}$$

where b is the "diffusion length," a material parameter typically in the range of one to three particle diameters. The idea behind Eq. (3) is that particles drift from regions of low to high downward velocity, where there are more local rearrangements (and more free volume) to accommodate their collective motion. The approximation of incompressibility, $\boldsymbol{\nabla}\cdot(\mathbf{u},-v)=0$, applied to Eq. (3) yields a diffusion equation for the downward velocity,

$$\frac{\partial v}{\partial z} = b\nabla_\perp^2 v, \tag{4}$$

where the vertical coordinate z acts like "time." Boundary conditions on Eq. (4) require no normal velocity component at the container walls, except at the orifice, where v is specified (effectively an "initial condition"). As described in the Appendix, this boundary-value problem can be accurately solved using a standard Crank-Nicholson scheme for the diffusion equation.

The kinematic parameter b can be understood as a diffusion length for free volume, which is introduced at the orifice

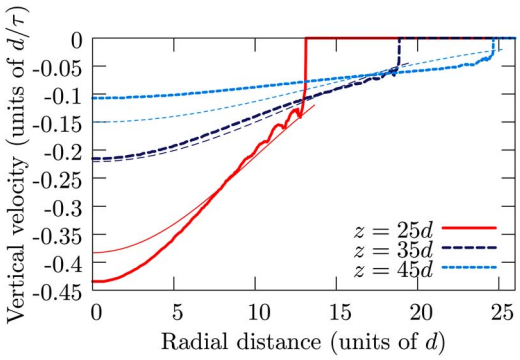

FIG. 5. (Color online) Velocity profiles for the 60° reactor geometry (heavy lines), with a comparison to the kinematic model for $b=3d$ (thin lines).

and diffuses upward, causing downward diffusion of particles. It was originally proposed that free volume is carried by voids [10,45], which displace single particles as they move, but a more realistic mechanism involves cooperative particle motion due to diffusing "spots" of delocalized free volume [17]. The spot model can produce accurate flowing packings in wide silos [18], and the kinematic model can be derived as the continuum limit of the simplest case where spots drift upward at constant velocity (due to gravity) while undergoing independent random walks, although more general continuum equations are also possible for different spot dynamics. A first-principles mechanical theory of spot dynamics is still lacking (although it may be based on a stochastic reformulation of Mohr-Coulomb plasticity [26]), so here we simply try a range of b values and compare to the DEM flow profiles.

Consistent with a recent experimental study of quasi-2D silos [9], we find reasonable agreement between the kinematic model predictions and the DEM flow profiles, but the effect of the container geometry is not fully captured. In the converging flow of the funnel region, the streamlines are roughly parabolic, as predicted by the kinematic model and found in many experiments [9,13–16]. For that region, it is possible to choose a single value ($b=3d$) to achieve an acceptable fit to the DEM flow profiles for both the 30° and 60° funnel geometries, as shown in Fig. 5.

In spite of the reasonable overall fit, the kinematic model has some problems describing the DEM results. It fails to describe the several particle thick boundary layer of slower velocities seen in the DEM data. In the original model, b depends only on the properties of the granular material, but we find that it seems to depend on the geometry; the best fit to the 30° DEM data is $b\approx 2.5d$, while the best fit for the 60° DEM data is $b\approx 3.0d$. Such discrepancies may partly be due to the boundary layers, since in the lower section of the container the conical walls may have an appreciable effect on the majority of the flow. We also find that the kinematic model fails to capture the rapid transition from converging flow to plug flow seen in the DEM data. This is shown clearly by comparing the streamlines for the kinematic model in Fig. 4 with those for DEM. Streamlines for the kinematic model are roughly parabolic, and no single value of b can capture the rapid change from downward

streamlines to converging streamlines seen in DEM.

The difficulty in precisely determining b is also a common theme in experiments, although recent data suggest that a nonlinear diffusion length may improve the fit [9]. Perhaps a more fundamental problem with the kinematic model is that it cannot easily describe the rapid crossover from parabolic converging flow to uniform plug flow seen in both geometries of our DEM simulations; we will return to this issue in Sec. V.

IV. DIFFUSION AND MIXING

Nuclear engineering codes for PBR core neutronics typically assume that pebbles flow in a smooth laminar manner along streamlines, with very little lateral diffusion [38,39]. Were such significant diffusion to occur across streamlines, it could alter the core composition in unexpected ways. In the MPBR design with a dynamic central column [8], diffusion leads to the unwanted mixing of graphite pebbles from the central reflector column with fuel pebbles from the outer annulus, so it must be quantified. Simulations and experiments are crucial, since diffusion in slow, dense granular flows is not fully understood [17].

Particle-tracking experiments on quasi-2D silos [16] and half-cylinder MPBR models [37] have demonstrated very little pebble diffusion in slow, dense flows, but the observations were made near transparent walls, which could affect the flow—e.g., due to ordering (see below). Three-dimensional tracking of a radioactive tracer in a cylindrical MPBR model has also shown very little diffusion, at the scale of a single pebble diameter for the duration of the flow [37]. Here, we take advantage of the complete information on pebble positions in our DEM simulations to study core diffusion and mixing with great accuracy.

We collected extensive statistics on how much pebbles deviate from the mean-flow streamlines during drainage. Consistent with theoretical concepts [17], experiments have demonstrated that the dynamics is strongly governed by the packing geometry, so that diffusion can most accurately be described by looking at the mean-squared horizontal displacement away from the streamline, as a function of the distance dropped by the pebble (not time, as in molecular diffusion), regardless of the flow rate. Motivated by the importance of quantifying mixing at the fuel/moderator interface in the dynamic central column of MPBR, we focus on tracking pebbles passing through $z=110d$ with $|r-15d| < 0.16d$. The variance of the r coordinate of the particles as they fall to different heights in z can be calculated. From this, we can determine the amount of radial diffusion, defined as the increase in the variance of r of the tracked particles from the variance at the initial height.

The diffusion data for both reactor geometries are shown in Fig. 6. We see that for large values of z in the cylindrical part of the container, the pebbles undergo essentially no diffusion; this is to be expected, since we have seen that in this area the packing is essentially plug like, and particles are locked in position with their neighbors. However, for lower values of z the amount of radial spreading begins to increase, as the particles experience some rearrangement in the region

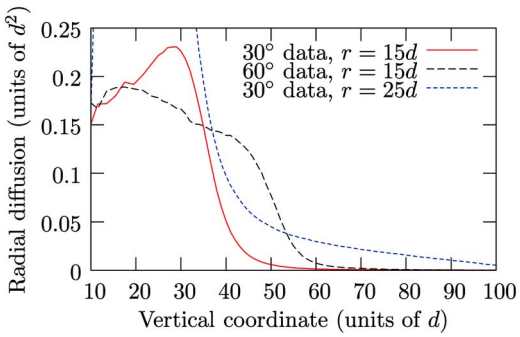

FIG. 6. (Color online) Radial diffusion of particles about streamlines of the mean flow as a function of height, z, in both reactor geometries for pebbles starting at $z=110d$ in an annulus of radius $r=15d$, at the edge of the dynamic central column in MPBR. For the 30° geometry, we also show data for pebbles near the wall at $r=25d$.

corresponding to converging flow. Note, however, that the scale of this mixing is very small and is much less than a pebble diameter. The height where the amount of diffusion begins to increase is approximately $z=35d$ in the 30° geometry and $z=50d$ in the 60° geometry. In the 30° geometry, this transition is significantly above the height of the interface between conical and cylindrical walls, while in the 60° geometry, the transition is almost level with the interface. This suggests that while the container geometry may play a role in diffusion and velocity profiles, it is a lower-order effect. For very small values of z, there is a decrease in the variance of the radial coordinate, since the pebbles must converge on the orifice as they exit the container.

We applied a similar analysis for different initial values of r and found very similar results over the range $0<r<25d$. However, for particles close to the container boundary, very different behavior is observed, as shown by the third line in Fig. 6 for particles with $|r-25d|<0.10d$. In this region, the particles undergo rearrangement, and this causes a (piecewise) linear increase in the mean-squared displacement with distance dropped, which corresponds to a constant local diffusion length. There is also evidence of a sharp transition in the boundary-layer diffusion length, which increases significantly as pebbles pass the corner into the converging-flow region of the funnel.

V. PACKING STATISTICS

A. Pebble volume fraction

Pebble-bed experiments [32,33] and simulations [40,41] of static sphere packings in cylinders have revealed that there are local variations in porosity near walls, at the scale of several pebble diameters, but there has been no such study of flowing packings, averaging over dynamic configurations. Similar findings would have important implications for helium flow in the core, since the local gas permeability is related to the porosity [34–36].

First, we study the distribution of local volume fraction (% of volume occupied by pebbles) throughout the container, averaged in time. (The porosity is 1 minus the volume

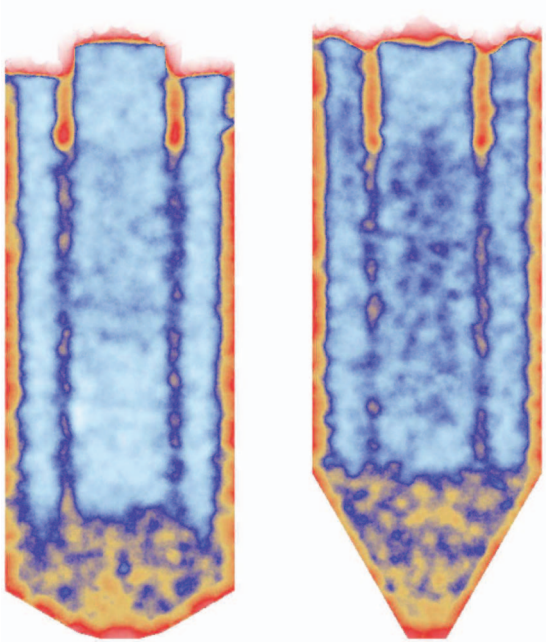

FIG. 7. (Color) Plots of local volume fraction (1−porosity) in a vertical cross section for the 30° reactor geometry (left) and the 60° reactor geometry (right), calculated using a Voronoi cell method. Volume fractions of 50%, 57%, 60%, and 63% are shown using the colors of red, yellow, dark blue, and cyan, respectively. Colors are smoothly graded between these four values to show intermediate volume fractions. High in the bulk of the container, the packing fraction is approximately 63%, apart from in a small region of lower density at $r_{in}=14.5d$, corresponding to packing defects introduced by the guide ring. In both geometries a sharp reduction in density is observed in a region above the orifice, where particles in the parabolic flow region are forced to undergo local rearrangements.

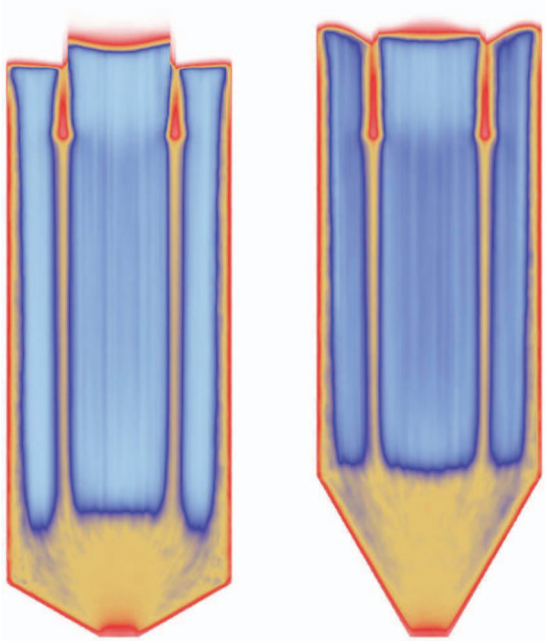

FIG. 8. (Color) Time-averaged plots of the local volume fraction, using the same color scheme as Fig. 7.

fraction.) Random close packing of spheres corresponds to a volume fraction in the range 55%–63%, while flows occur in a somewhat more restricted range. The lower bound is approximately set by random loose packing, where rigidity percolation sets [46], while the upper bound is near the jamming point [47] or the maximally random jammed state [48], where flow cannot occur.

The best way to determine the volume fraction on a local scale is to use a Voronoi tessellation, which uniquely assigns a polygonal volume to each pebble, formed by intersecting the planes bisecting the lines between different pebble centers. Widely used algorithms (such as the one found in MATLAB) compute Voronoi cells using the dual Delaunay tessellation, but our algorithm efficiently computes the Voronoi cells directly, plane by plane. One of the advantages of this direct method (to be described in detail elsewhere) is that it allows us to approximate the Voronoi cells of particles near the walls with a high degree of accuracy by cutting the Voronoi cell with the appropriate planes. The local packing fraction in a small region can be found by taking the ratio of the particle volume in that region to the ratio of the Voronoi volume. Such a method can be used to define local density even down to the scale of a single particle, but for this work we compute local density by averaging on a scale of several particle diameters.

Figure 7 shows density snapshots for cross sections through the 30° and 60° reactor geometries, based on computing the local density at a particular point by averaging over the Voronoi densities of particles within a radius of $2.2d$. Figure 8 shows density plots over the entire flow of the data, but using a smaller averaging radius of $0.8d$. Many interesting features are visible, which corroborate our other results. High in the center of the container, we see that the local packing fraction is mostly close to 63%, suggesting that the pluglike region is in a nearly jammed and rigid state. This is consistent with our earlier data showing nearly uniform plug flow with no significant diffusion or mixing.

We also observe two annular lines of lower density propagating down from the guide ring, which form due to wall effects on the guide ring itself (see below) and are advected downward. The fact that these subtle artifacts of the guide-ring constraints are felt far down in the flow further demonstrates that very little diffusion or shearing occurs in the upper region. There are also similar lower-density regions along the walls, related to partial crystallization described in more detail below.

It is also clear in both geometries, especially the 30° model, that there is a fairly sharp transition between the upper region of nearly rigid plug flow and a less dense lower region of shear flow in the funnel. Similar features are in the velocity profiles described above, but the transition is much more sharp, at the scale of at most a few particles, for the local packing fraction. These sudden variations in material properties and velocities are reminiscent of shocklike discontinuities in Mohr-Coulomb plasticity theories of granular materials [12,24]. It seems no such existing theory can be applied to the reactor flows, but our results suggest that plasticity concepts may be useful in developing a continuum theory of dense granular flow [26].

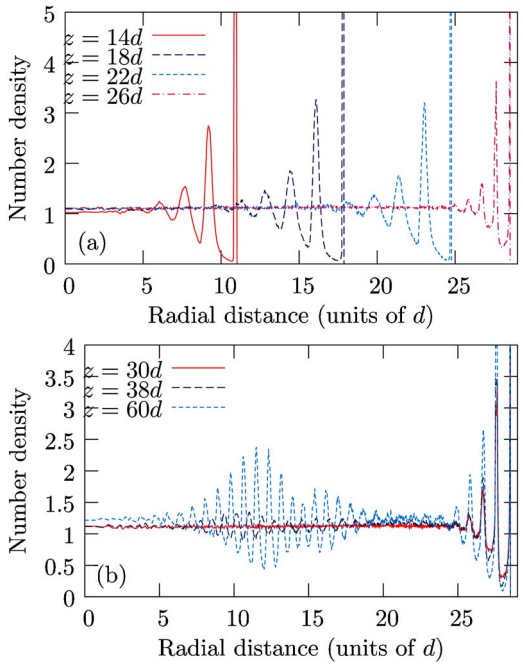

FIG. 9. (Color online) Number density plots in the 30° reactor geometry for several low cross sections (a) and several high cross sections (b).

B. Local ordering and porosity

As noted above, previous simulation studies of local ordering near walls have focused on static packings in simplified cylindrical geometries (without the funnel, outlet pipe, or guide ring) [40,41], while we compute average statistics for slowly flowing packings in realistic full-scale reactor models. To take a closer look at ordering near walls, we study the number density profile in horizontal slices at different heights. The container is divided into bins in the same way as discussed previously and the number density in a bin is obtained by counting the number of times a particle center lies within that bin.

Figure 9(a) shows a sequence of number density profiles for several low values of z in the 30° reactor geometry. At all four heights, lattice effects are clearly visible and quite similar to those observed in experiments [32,33] and other simulations [40,41]. For the lowest three heights, these peaks are roughly $\sqrt{3}d$ apart, corresponding to particles crystallized against the conical wall, while for the highest value of z, these effects are roughly $1d$ apart, due to particles being crystallized against the cylindrical wall. The graph also shows that in the middle of the container, no lattice effects are present.

However, this situation changes dramatically higher up in the container, as shown in Fig. 9(b). As z increases from $30d$ to $60d$, the interior of the packing goes from being disordered to having a strong radial ordering, centered at around $z=12d$. The reason for this ordering is due to the presence of the guide ring high in the container, which keeps the fuel and moderator pebbles separate. The ring, placed at $r_{\text{in}}=14.5d$ in the container, creates radial crystallization, which can then propagate very far downward, since the packing is plug like

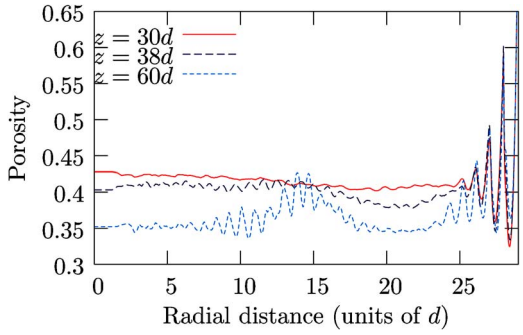

FIG. 10. (Color online) Horizontal profiles of porosity at different heights in the 30° reactor geometry.

for most of the cylindrical part of the reactor. At much lower heights, around $z=40d$, this radial ordering is broken, as the particles are forced to reorganize once they enter the parabolic region of flow.

To make a direct connection with the modeling of gas flow, we show horizontal slices of the porosity at different heights in Fig. 10. The porosity is measured here by intersecting the spheres with annular cylindrical bins to compute the fraction of each bin volume not occupied by pebbles. The features noted above appear in the porosity and alter the local permeability, which enters continuum descriptions of helium gas flow in the core [34–36].

VI. RESIDENCE-TIME DISTRIBUTION

A. Predictions of the kinematic model

The statistical distribution of fuel burn-up is closely related to the distribution of pebble residence times in the reactor core, differing only due to nonuniform sampling of the neutron flux profile. Since the upper pebble flow is essentially a uniform plug flow, the distribution of residence times is the same (up to a constant time shift) as the distribution of waiting times for pebbles starting at a given height in the core to exit through the orifice, and we concentrate on these distributions in this section. However, we conclude by examining the residence times for particles to pass through the entire container, to investigate the effects of the guide ring and the outer walls.

We have seen that there is very little pebble diffusion, so fluctuations in the residence time are primarily due to hydrodynamic dispersion in the mean flow. We have also seen that the kinematic model gives a reasonable description of the mean flow profile in the conical funnel region, where most of the shear and hydrodynamic dispersion occur. Therefore, we can approximate the residence-time distribution by the distribution of times to travel along different streamlines of the mean flow, starting from different radial positions r_0 at a given height z_0. Below we will compare such predictions, based on our numerical solutions to the kinematic model, to our DEM simulations for the two reactor geometries.

B. Analytical formula

We can obtain a simple, exact formula for the residence-time distribution in a somewhat different geometry using the

kinematic model, as follows. The similarity solution to Eq. (4) for a wide, flat-bottomed silo draining to a point orifice at $z=0$ is

$$u(r,z) = -\frac{Qr}{2bz^2}e^{-r^2/4bz}, \tag{5}$$

$$v(r,z) = \frac{Q}{bz}e^{-r^2/4bz}, \tag{6}$$

where u and v are the radial (horizontal) and downward velocity components and Q is a constant proportional to the total flow rate through the orifice. (This is just the classical Green function for the diffusion equation in two dimensions, where z acts like "time.") A slightly more complicated solution is also possible for a parabolic silo, but let us focus on the simplest case of Eqs. (5) and (6), which is a good approximation for a wide parabolic funnel, where the velocity near the walls is small—i.e., $R > \sqrt{4bz_0}$. A more detailed analysis is not appropriate here, since a simple analytical solution does not exist for the actual reactor geometry of a conical funnel attached to straight cylinder.

For the flow field in Eqs. (5) and (6), the trajectory of a Lagrangian tracer particle along a streamline is given by

$$\frac{dr}{dt} = u(r,z), \quad r(t=0) = r_0, \tag{7}$$

$$\frac{dz}{dt} = -v(r,z), \quad z(t=0) = z_0. \tag{8}$$

Combining these equations and integrating, we find that the streamlines are parabolas, $z/z_0=(r/r_0)^2$, and that the residence time for a pebble starting at (r_0,z_0) is

$$\tau_0(r_0,z_0) = \frac{bz_0^2}{2Q}e^{r_0^2/4bz_0}. \tag{9}$$

Now we consider pebbles that are uniformly distributed at a height z_0 in a circular cross section of radius R in the flow field Eqs. (5) and (6). The probability distribution for the residence time of those pebbles is

$$p(\tau|z_0,R) = \int_0^R \delta(\tau - \tau_0(r_0,z_0))\frac{2\pi r_0 dr_0}{\pi R^2} \tag{10}$$

$$= \begin{cases} 0 & \text{for } \tau < \tau_{min}(z_0), \\ 4bz_0/R^2\tau & \text{for } \tau_{min} < \tau < \tau_{max}, \\ 0 & \text{for } \tau > \tau_{max}(z_0,R), \end{cases} \tag{11}$$

where

$$\tau_{min} = \tau_0(0,z_0) = \frac{bz_0^2}{2Q}, \tag{12}$$

$$\tau_{max} = \tau_0(R,z_0) = \frac{bz_0^2}{2Q}e^{R^2/4bz_0}. \tag{13}$$

Once again, this solution is strictly valid for an infinitely wide and tall silo draining to a point orifice, and it is roughly valid for a parabolic funnel, $z/z_0=(r/R)^2$, as an approximation of a conical funnel in the actual reactor geometry. We can further approximate the effect of a nearly uniform flow of speed v_0 to describe the upper cylindrical region by simply adding $(z-z_0)/v_0$ to the residence time for a starting point $z>z_0$.

Although this analysis is for a modified geometry, we will see that it captures the basic shape of the residence-time distributions from the DEM simulations in a simple formula (11). The probability density is sharply peaked near the shortest residence time τ_{min}, corresponding to pebbles near the central axis traveling the shortest distance at the largest velocity. The longer distance and (more importantly) the smaller velocity at larger radial positions cause strong hydrodynamic dispersion, resulting a fat-tailed residence-time density which decays like $1/t$, up to a cutoff τ_{max}.

C. Simulation results

For the DEM reactor simulations, we calculate the distribution of times it takes for particles to drop from several different values of z_0, adding in a weighting factor to take into account that shorter residence times are preferentially observed in the data set.

Since we are primarily interested in the radioactive burnup, we concentrate on the residence times for the fuel pebbles, but for comparison, we also report results for the moderator pebbles. Figure 11(a) shows the residence-time probability densities for pebbles starting at $z=40d,55d,70d$ to exit the container for the 30° reactor geometry. The distributions for the moderator pebbles are quite narrow, showing that all particles exit over a short time window. In contrast, the distributions for the fuel pebbles exhibit fat tails, as expected qualitatively from the kinematic model approximation (11) for a parabolic geometry. A closer analysis of the data confirms that the longest waiting times are associated with pebbles passing close to the walls, especially near the corner between the conical and cylindrical wall sections, although there are no completely stagnant regions.

Figure 11(b) shows corresponding plots for the 60° reactor geometry. In general, the residence-time densities have similar shapes as for the 30° geometry, but they are much narrower and exhibit a small secondary peak far into the tail. Examining movies shows that this extra peak is due to a boundary layer of particles, roughly one-pebble thick, touching the 60° conical wall sliding down at a speed lower than the nearby bulk. This extra source of hydrodynamic dispersion could not be easily captured by a continuum model for the mean flow. A simple way to eliminate it would be to replace add an outer annulus of moderator pebbles (controlled by another guide ring at the top), which would flow more slowly along the walls, leaving the fuel pebbles in a more uniform flow with smaller fluctuations. Another possibility would be to reduce the wall friction, which makes the

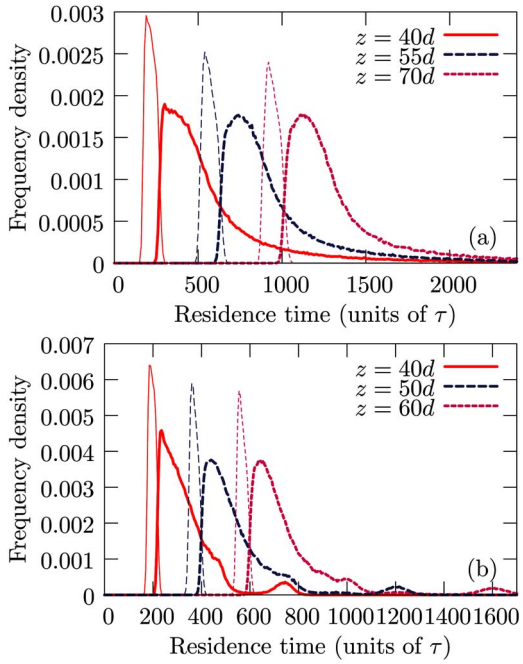

FIG. 11. (Color online) Residence-time probability densities for the time it takes particles to drop from a specific height z out of the container, for the 30° reactor geometry (a) and 60° reactor geometry (b) for fuel pebbles (heavy lines) and for moderator pebbles (thin lines).

flow more uniform, as discussed in the following section.

Figure 12 investigates the accuracy of the kinematic model in predicting the DEM residence-time distribution. The total residence-time distribution for both fuel and moderator pebbles to exit the reactor from $z=40d$ in the 30° geometry is shown and is compared with two predictions from the kinematic model, one making use of the analytic formula (11) and one making use of the numerical solution of the velocity profile. We use of the value $b=2.5d$ and calibrate the total flow to match the total flow from the DEM data. Both the numerical solution and the analytic formula can roughly capture the overall shape of the DEM distribution, although neither achieves a good quantitative agreement, particularly in the tails. Since the analytic formula assumes all streamlines are parabolic, it fails to take into

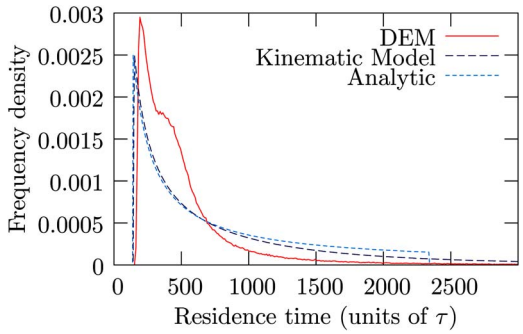

FIG. 12. (Color online) Comparison of the residence time distributions between DEM simulation, numerical solution of the kinematic model, and the analytic formula.

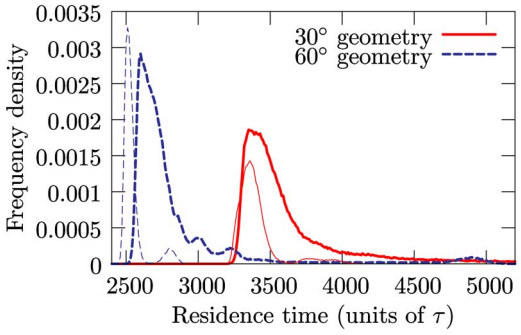

FIG. 13. (Color online) Distribution of times to pass through the entire container for fuel pebbles (heavy lines) and moderator pebbles (thin lines).

account the slow-moving particles that stay close to the wall, and it therefore predicts a cutoff in the residence-time distribution which is much shorter than some of the observed residence times in the DEM simulation. The numerical solution of the kinematic model accounts for this and provides a better match, although it is clear that a model correctly accounting for the flow of pebbles near the container walls may be required in order to achieve high accuracy.

D. Residence times for the entire container

We also considered the distribution of times for the particles to pass through the entire container. While the flow in the upper part of the reactor is essentially plug like, boundary effects near the container walls and on the guide ring can have an appreciable effect on the pebble residence times, which we study here. Since it takes a long time for particles to pass through the entire container, we made use of the two extended data sets, consisting of 1427 snapshots for the 30° geometry and 1249 snapshots for the 60° geometry.

Figure 13 shows the time distributions for pebbles to pass through the entire container. Apart from a large positive time shift, the curves are similar in form to those in Fig. 11. However, for both geometries, we see second small peaks in the distributions for the moderator pebbles, corresponding to a slow-moving boundary layer of pebbles touching the guide ring. The 60° curve for the fuel pebbles also exhibits several undulations corresponding to multiple layers of pebbles crystallized against the outer wall, each moving at different speeds.

VII. WALL FRICTION

The behavior of pebbles near the walls is of significant interest to reactor design, and to look into this further, we investigated the effect of wall friction by comparing two simulation runs in the half-size geometry, with wall friction coefficients $\mu_w=0$ and $\mu_w=0.7$. All other aspects of the simulation, including the interparticle interactions, were kept the same.

Figures 14 and 15 show comparisons of flow streamlines and velocity profiles, respectively, for the two simulations. We see that the $\mu_w=0$ simulation results in a significantly larger flow speed, with a mass flow rate of $104\tau^{-1}m$, as

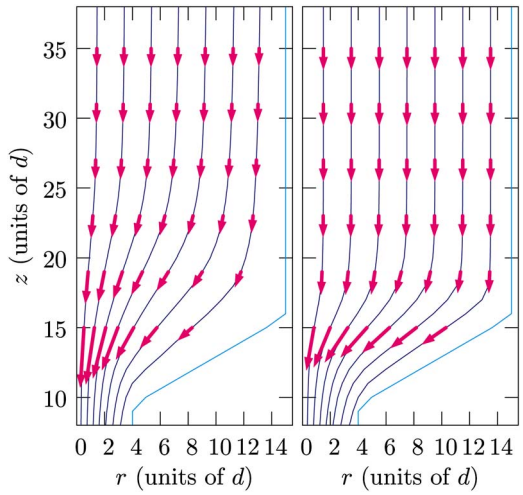

FIG. 14. (Color online) Streamlines for the half-size, monodisperse geometries with wall friction (left) and without wall friction (right). Arrows are proportional to the velocity vectors in selected horizontal slices.

opposed to $59.6\tau^{-1}m$ for $\mu_w=0.7$. As would be expected, removing wall friction also removes the boundary layer of slower velocities at the wall, creating an almost perfectly uniform velocity profile high in the reactor. This also has the effect of increasing radial ordering effects, and we can see from Fig. 16 that the number density profile is more peaked close to the wall. Figure 16 also shows that the radial ordering created by the guide ring is also significantly enhanced. While this is due in part to the more pluglike flow allowing packing effects to propagate further down, it is also due to the frictionless guide ring initially creating radial ordering. Thus it may be possible to tune the material properties of the guide ring (or the roughness of its walls) to enhance or reduce the radial ordering effects.

Removing wall friction also has the effect of increasing radial ordering effects near the wall. Perhaps most surprisingly, removing wall friction results in a significant alteration of the flow in the *interior* of the packing, as shown by the two velocity profiles in Fig. 15 for $z=18d$. While both velocity profiles must converge upon the orifice, we see that the velocity profile for the $\mu_w=0.7$ case is significantly more curved than that for $\mu_w=0$. This also has the effect of

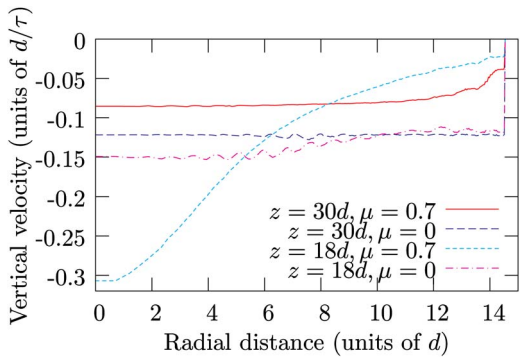

FIG. 15. (Color online) Comparison of velocity profiles for simulations with and without wall friction for two different heights.

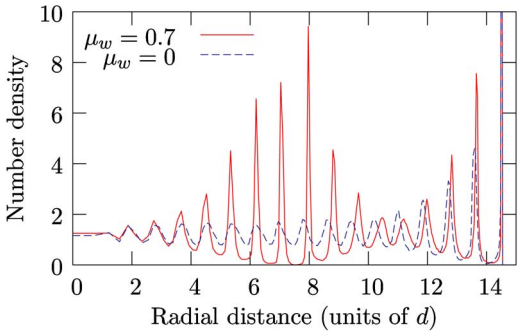

FIG. 16. (Color online) Comparison of number density profiles at $z=60d$ for simulations with and without wall friction.

preferentially speeding up the relative flux of fuel pebbles: with wall friction, the fuel pebbles make up 71.5% of the total mass flux, but without wall friction, this increases to 74.7%.

VIII. BIDISPERSITY

A. Bidisperse PBR concept

The two-pebble design of MPBR with a dynamic central moderator column has various advantages over a solid graphite central column (as in the revised PBMR design). For example, it flattens the neutron flux profile, while preserving a very simple core vessel without any internal structures, which would be subjected to extreme radiation and would complicate the granular flow. It also allows the widths of the moderator column and fuel annulus to be set "on the fly" during reactor operation, simply by adjusting the guide ring at the top.

A drawback of the dynamic moderator column, however, is its porosity, which allows the passage of the helium gas coolant, at the highest velocity (along the central axis). In most PBR designs, high-pressure helium gas is introduced from a reservoir above the core, through holes in the graphite bricks which make up the core vessel. The gas then flows through the core and exits through holes in the graphite bricks of the conical funnel to another reservoir at high temperature. To improve the thermal efficiency and power output, it would be preferable to focus the gas flow on the fuel annulus and the interface with the moderator column, where the most heat is generated. This is automatically achieved with a solid graphite column, but there is a very simple way to shape the gas flow in a similar way with a dynamic column, while preserving its unique advantages.

The idea is to make the graphite moderator pebbles in the central column smaller than the fuel pebbles in the outer annulus, as shown in Fig. 17. (This also helps with sorting of fuel and moderator pebbles as they exit the core.) In standard continuum models of flow in porous media [34–36], the permeability of the packing scales with the square of the pebble diameter (or pore size), so reducing the diameter of the moderator pebbles can greatly reduce the gas flow (e.g., by a factor of 4 for half-diameter pebbles). This argument holds everywhere that the packing is statistically the same, in the monodisperse packings of the fuel annulus and the modera-

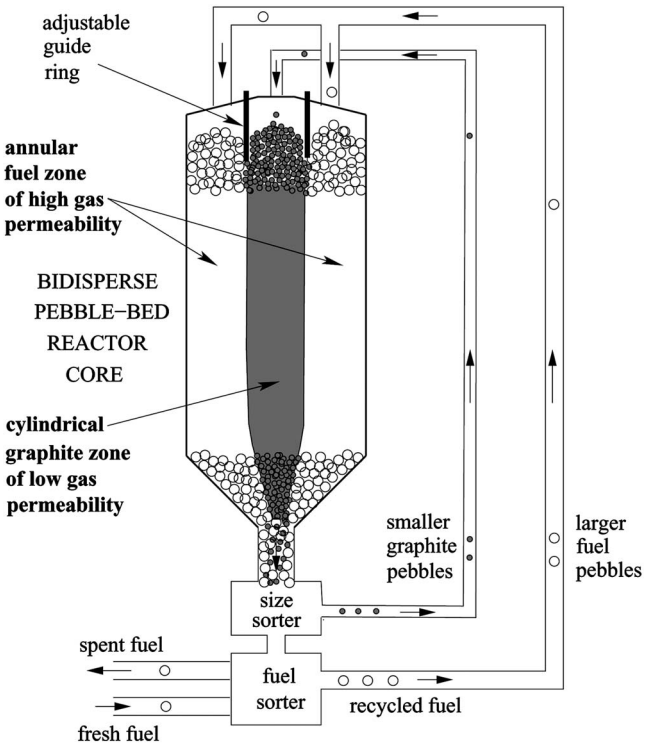

FIG. 17. Schematic diagram of the pebble flow in a bidisperse MPBR design.

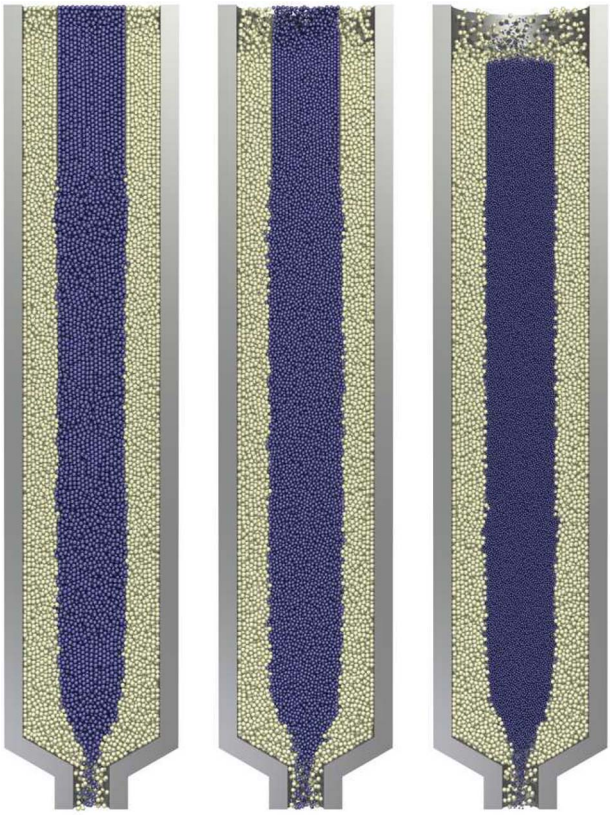

FIG. 18. (Color online) Snapshots of vertical cross sections for the bidisperse simulations. From left to right, the moderator pebbles have diameters $1d$, $0.8d$, and $0.5d$ while the fuel pebbles are of constant size $1d$.

tor column, which have the same porosity. At the interface between the two regions, we have seen in Figs. 7 and 10 that the porosity is enhanced for a monodisperse core due to the guide ring, although a bidisperse interface will have different structure. In summary, if helium gas is introduced outside the guide ring in a bidisperse core, it can be made to pass almost entirely through the fuel annulus and the interface with the moderator column.

B. Simulation results

The only question regarding the feasibility of the bidisperse core is the stability of the central column over time and the possibility of enhanced diffusion of the small moderator pebbles into the annulus of larger fuel pebbles. In other systems, such as rotating drums [49–51], vibrated buckets [52,53], and draining silos [15], bidisperse granular materials display a tendency to segregate (rather than mix) during dynamics, but there is currently no general theory which could be applied to our reactor geometry. Therefore, our DEM simulations provide a useful means to address this important question.

Figure 18 shows snapshots of vertical cross sections for the three different bidisperse simulations that were run in the half-size geometry. As shown in the diagram, the central column remains stable and coherent in all three cases, and very little mixing between the two types of pebbles is visible. Figure 19 shows a comparison of the velocity profiles from the three simulations for two different heights. It is reassuring to see that the bidisperse simulations do not significantly differ from the monodisperse simulation, although we do see a slightly higher overall flow rate in the bidisperse systems: we see total mass flow rates of $59.6\tau^{-1}m$, $60.8\tau^{-1}m$, and $65.0\tau^{-1}m$ for the monodisperse, 0.8:1, and 0.5:1 simulations, respectively.

The velocity profiles are slightly more curved in the bidisperse central core; this is particularly apparent in the 0.5:1 simulation. This leads to a small cusp in the velocity profile near the interface between the two types of particles which may lead to adverse mixing effects. The faster flow also leads to a significantly larger turnaround of the modera-

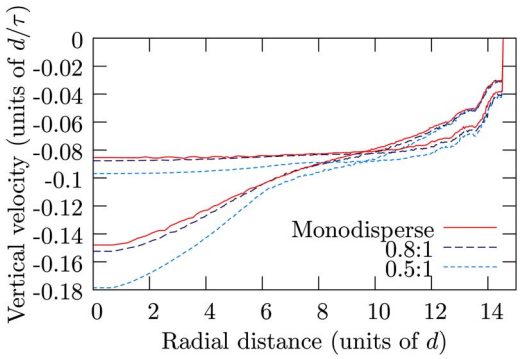

FIG. 19. (Color online) Comparison of velocity profiles for the three bidisperse simulations. The three flatter curves are calculated at $z=30d$ in the pluglike flow region while the other three were taken at $z=22d$ in the parabolic flow region.

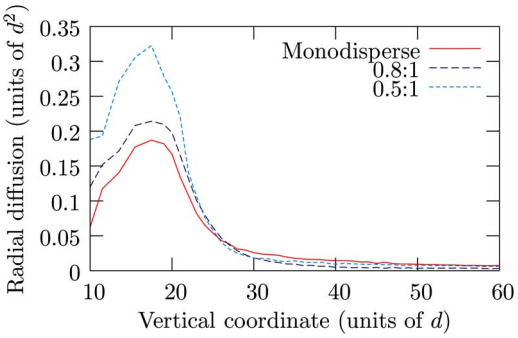

FIG. 20. (Color online) Comparison of particle diffusion for the three bidisperse simulations.

tor pebbles. In the monodisperse system, the moderator pebbles comprise 28.5% of the total mass flux, but this is increased to 31.7% in the 0.8:1 bidisperse simulation and 42.6% in the 0.5:1 bidisperse simulation.

To investigate the amount of mixing of the central column, we used a technique similar to that described in Sec. IV. At $z=110d$ all moderator particles with $r>8d$ are marked and their radial diffusion is then calculated as a function of z. The results are shown in Fig. 20: in the cylindrical section of the packing, there is very little difference between the three simulations, but in the area of convergent flow, we see that bidispersity leads to significantly more mixing. However, even for the 0.5:1 simulation, the scale of diffusion is still smaller than a single particle diameter and essentially the central column remains stable.

Due to computational limitations, we were unable to investigate smaller size ratios in the reactor geometries, so we carried out simulations in a smaller container with a 0.3:1 size ratio and found dramatically different behavior: During drainage, the central column became unstable and the small particles penetrated many particle diameters into the packing of larger particles. We expect that there is a fundamental crossover in behavior simply due to geometry of amorphous packings, when the moderator pebbles become small enough to pass through the gaps between the densely packed fuel pebbles. An in-depth study of this phenomenon remains a subject of future work. For now, we can safely recommend a diameter ratio of 0.5:1, which reduces the dynamic central column's permeability by a factor of 4 without introducing any significant diffusion of moderator pebbles into the fuel annulus.

IX. CONCLUSIONS

A. Pebble-bed reactor core design

Using DEM simulations, we have analyzed many aspects of granular flow in pebble-bed reactor cores of direct relevance for design and testing. We close by summarizing some key conclusions.

The mean flow profile exhibits a smooth transition from a nearly uniform plug flow in the upper cylindrical region to a nonuniform, converging flow in the lower funnel region, consistent with recent experiments [9,37]. There are no stagnant regions in the 30° and 60° conical funnels considered in this study, although the flow is slower near the corner at the top of the funnel, especially in the former case. Moreover, the wider 30° funnel has a boundary monolayer of slower pebbles partially crystallized on the wall.

The only available continuum theory for such flows, the simple kinematic model [10–12,45], gives a reasonable qualitative picture of the flow profiles, although it cannot capture discrete boundary-layer effects. As in other experiments on similar geometries [9], the kinematic model does not quantitatively predict the dependence of the flow profile on geometry. We suggest that it be used to get a rough sense of the flow profile for a given core geometry prior to (much more computationally expensive) DEM simulations and/or experiments.

We have quantified the degree of pebble mixing in the core. Although there is some horizontal diffusion in the funnel region, pebbles depart from the streamlines of the mean flow by less than one pebble diameter prior to exiting the core.

We have demonstrated that the "mixing layer" between the central moderator column and the outer fuel annulus, which appears in prior models [39], can be reduced to the thickness of one pebble diameter by separating moderator and fuel pebbles with a guide ring at the ceiling (to eliminate mixing by surface avalanches), consistent with experiments on MPBR models [37]. We conclude that the dynamic central column of moderator pebbles is a sound concept, which should not concern regulators.

We have constructed Voronoi tessellations of our flowing packings to measure the profile of volume fraction (or porosity) and found some unexpected features which would affect coolant gas flow through the core. The bulk of the core, in the plug-flow region of the upper cylinder, has a volume fraction near the jamming point (63%), but there is a sharp transition to less dense packings (55%–60%) in the funnel region, due to shear dilation. We also observe lower volume fractions in this range at the moderator/fuel interface in the upper cylinder, below the guide ring, and lower volume fractions (50%–55%) against the walls. These narrow regions of increased porosity (and thus, increased permeability) would allow faster helium gas flow.

We have also studied local ordering in the flowing packings and find evidence for partial crystallization within several pebble diameters of the walls, consistent with previous experiments [32,33] and simulations [40,41]. Such ordering on the walls of the guide ring, then advected down through the core, is responsible for the increased porosity of the moderator/fuel interface.

We have varied the wall friction in our DEM simulations and observe that it can affect the mean flow, even deep into the bulk. Reducing the wall friction increases radial ordering near the walls and makes the flow profile more uniform.

Since diffusion is minimal, the probability distribution of pebble residence times is dominated by advection in the mean flow. Therefore, we have made predictions using the kinematic model, numerically for the conical-funnel reactor geometries and analytically for a wide parabolic funnel. The model predicts a fat-tailed ($\sim 1/t$) decay of the residence-time density due to hydrodynamic dispersion in the funnel region.

Our DEM simulations predict that the 60° conical funnel results in a narrower residence-time distribution than the 30° funnel, which has more hydrodynamic dispersion. The steeper 60° funnel also exhibits a boundary layer of slower, partially crystallized pebbles near the wall which lead to an anomalous bump far in the tail of residence-time distribution. These results have important implications for nonuniformity in the burn-up of fuel pebbles.

We have introduced the concept of a bidisperse core with smaller moderator pebbles in the dynamic central column than in the outer fuel annulus, in order to focus the helium gas flow on the fuel. Our DEM simulations demonstrate that there is negligible pebble mixing at the interface for diameter ratios as small as 0.5:1, for which the permeability of the moderator column is reduced by a factor of 4. We conclude that the bidisperse MPBR design is sound and will produce a stable moderator-pebble column of greatly reduced gas permeability.

A natural next step would be to combine our full-scale DEM model for the pebble flow with existing computational approaches to reactor core physics [38,39], which rely on pebble flow as an empirical input. More accurate studies of gas flow in the core could also be done, starting from our complete pebble packings or the average quantities such as the porosity. With such computational tools, one should be able to reliably test and develop new reactor designs.

B. Basic physics of dense granular flow

We have noted a number of favorable comparisons between our simulations and experiments in similar geometries [9,32,33,37], which provides further validation of the discrete-element method as a realistic means of simulating granular materials. As such, it is interesting to consider various implications of our results for the theories of dense granular flow, since the simulations probe the system at a level of detail not easily attained in experiments.

Our conclusions about the kinematic model are similar to those of a recent experimental study [9]: The model describes the basic shape of the flow field in the converging region, but fails to predict the nearly uniform plug flow in the upper region with vertical walls or the precise dependence on the funnel geometry. It also cannot describe boundary layers due to partial crystallization near walls or incorporate wall friction, which we have shown to influence the entire flow profile.

On the other hand, there is no other continuum model available for dense silo drainage, except for Mohr-Coulomb plasticity solutions for special 2D geometries, such as a straight 2D wedge without any corners [12], so it is worth trying to understand the relative success of the kinematic model for our 3D reactor geometries and how it might be improved. A cooperative microscopic mechanism for random-packing dynamics, based on "spots" of diffusing free volume, has recently been proposed, which yields the mean flow of the kinematic model as the special case of independent spot random walks with uniform upward drift from the orifice (due to gravity) [17]. Under the same assumptions, the spot model has also been shown to produce rather realistic simulations of flowing packings in wide silos (compared to DEM simulations) [18], where the kinematic model is known to perform well [13–16]. This suggests that some modification of the spot dynamics, such as spot interactions and/or nonuniform properties coupled to mechanical stresses and an associated modification of the kinematic model in the continuum limit, may be possible to better describe general situations.

From a fundamental point of view, perhaps the most interesting result is the profile of Voronoi volume fraction (or porosity) in our flowing random packings in Fig. 7. Although the mean velocity in Fig. 2 shows a fairly smooth transition from the upper plug flow to the lower converging flow, the volume fraction reveals a sharp transition (at the scale of one to three particles) from nearly jammed "solid" material in the upper region (63%) to dilated, sheared "liquid" material in the lower region (57%–60%). The transition line emanated from the corners between the upper cylinder and the conical funnel. We are not aware of any theory to predict the shape (or existence) of this line, although it is reminiscent of a "shock" in the hyperbolic equations of 2D Mohr-Coulomb plasticity [12].

Our measurements of diffusion and mixing provide some insights into statistical fluctuations far from equilibrium. Consistent with the experiments in wide quasi-2D silos [16], we find that diffusion is well described geometrically as a function of the distance dropped, not time (as in the case of thermal molecular diffusion). As a clear demonstration, there is essentially no diffusion as pebbles pass through the upper core, until they cross the transition to the funnel region, where the diffusion remains small (at the scale of one pebble diameter) and cooperative in nature. The behavior in the funnel is consistent with the basic spot model [17], but a substantial generalization would be needed to describe the transition to the upper region of solidlike plug flow, perhaps using concepts from plasticity theory [26].

We view silo drainage as a fundamental unsolved problem, as interesting and important as shear flow, which has received much more attention in physics. The challenge will be to find a single theory which can describe both shear cells and draining silos. Our results for pebble-bed reactor geometries may provide some useful clues.

ACKNOWLEDGMENTS

This work was supported by the U.S. Department of Energy (Grant No. DE-FG02-02ER25530) and the Norbert Weiner Research Fund and the NEC Fund at MIT. Work at Sandia was supported by the Division of Materials Science and Engineering, Basic Energy Sciences, Office of Science, U.S. Department of Energy. Sandia is a multiprogram laboratory operated by Sandia Corporation, a Lockheed Martin Company, for the U.S. Department of Energy's National Nuclear Security Administration under Contract No. DE-AC04-94AL85000.

APPENDIX: NUMERICAL SOLUTION OF THE KINEMATIC MODEL

In the kinematic model for drainage the vertical downward velocity u in the container is assumed to follow a diffusion equation of the form

$$\frac{\partial v}{\partial z} = b\nabla_\perp^2 v,$$

where $\nabla_\perp^2$ is the horizontal Laplacian. By exploiting the axial symmetry, v can be treated as a function of z and r only. In cylindrical coordinates the Laplacian is

$$\frac{\partial v}{\partial z} = b\frac{1}{r}\frac{\partial}{\partial r}\left(r\frac{\partial v}{\partial r}\right)$$

$$= b\frac{\partial^2 v}{\partial r^2} + b\frac{1}{r}\frac{\partial v}{\partial r}.$$

The radial velocity component is given by

$$u = b\frac{\partial v}{\partial r},$$

and by enforcing that the velocity field at the wall must be tangential to the wall, we can obtain boundary conditions for solving v.

To solve the above equation in a cylinder is straightforward, since we can make use of a rectangular grid. The boundary condition reduces to $v_r=0$ at the wall. However, to solve this equation in the reactor geometry, we must also consider the complication of the radius of the wall, R, being a function of z. To ensure accurate resolution in the numerical solution of v at the wall, we introduce a new coordinate $\lambda=r/R(z)$, $\eta=z$, which then allows us to solve for u over the range $0<\lambda<1$. Under this change of variables, the partial derivatives transform according to

$$\frac{\partial}{\partial r} = \frac{1}{R(\eta)}\frac{\partial}{\partial \lambda},$$

$$\frac{\partial}{\partial z} = \frac{\partial}{\partial y} - \frac{\lambda R'(\eta)}{R(\eta)}\frac{\partial}{\partial \lambda}.$$

In the transformed coordinates,

$$R^2 v_\eta = \frac{b}{\lambda}v_\lambda + bv_{\lambda\lambda} + \lambda RR' v_\lambda.$$

To ensure differentiability at $r=0$, we use the boundary condition

$$\left.\frac{\partial v}{\partial \lambda}\right|_{\lambda=0} = 0, \tag{A1}$$

and by ensuring zero normal velocity at the wall we find that

$$\left.\frac{\partial v}{\partial \lambda}\right|_{\lambda=1} = -\frac{vR'R}{b}. \tag{A2}$$

To numerically solve this partial differential equation, we make use of the implicit Crank-Nicholson integration scheme. We write $v_j^n = v(j\Delta\lambda, n\Delta\eta)$ and solve in the range $j=0,1,\ldots,N$ where $N=\Delta\lambda^{-1}$. Away from the end points, the Crank-Nicholson scheme tells us that

$$\frac{v_j^{n+1}-v_j^n}{\Delta\eta} = \frac{b}{2\Delta\lambda^2 R^2}(v_{j+1}^{n+1} - 2v_j^{n+1} + v_{j-1}^{n+1} + v_{j+1}^n - 2v_j^n + v_{j-1}^n)$$
$$+ \left(\frac{b}{4j\Delta\lambda^2 R^2} + \frac{jR'}{4R}\right)(v_{j+1}^{n+1} - v_{j-1}^{n+1} + v_{j+1}^n - v_{j-1}^n),$$

where all references to R and R' are evaluated at $\eta=\Delta\eta\left(j+\frac{1}{2}\right)$. If $j=0$, then by reference to Eq. (A1), we find that

$$\frac{v_0^{n+1}-v_0^n}{\Delta\eta} = \frac{b}{\Delta\lambda^2 R^2}(v_1^{n+1} - v_0^{n+1} + v_1^n - v_0^n).$$

Similarly, for $j=N$, by reference to Eq. (A2), we see that effectively

$$\frac{v_{N+1}^n - v_{N-1}^n}{2\Delta\lambda} = -\frac{v_N^n R'R}{b}$$

and hence

$$\frac{v_N^{n+1}-v_N^n}{\Delta\eta} = \frac{b}{\Delta\lambda^2 R^2}(v_{N-1}^{n+1} - v_N^{n+1} + v_{N-1}^n - v_N^n)$$
$$- \left(\frac{(2N+1)R'}{2R} + \frac{R'^2}{2b}\right)(v_N^{n+1} + v_N^n).$$

If we write $\mathbf{v}^n=(v_0^n, v_1^n, \ldots, v_N^n)^T$, then the above numerical scheme can be written in the form $S\mathbf{v}^{n+1}=T\mathbf{v}^n$ where S and T are tridiagonal matrices; this system can be efficiently solved by recursion in $O(N)$ time. The above scheme was implemented in C++ and gives extremely satisfactory results, even with a relatively small number of grid points.

[1] See, e.g., http://gif.inel.gov, http://nuclear.inel.gov
[2] K. Fukuda *et al.* (unpublished).
[3] D. Nicholls, Nucl. News (La Grange Park, Ill.) **44**, 3 (2001).
[4] D. Talbot, MIT Technol. Rev. **105**, 54 (2002).
[5] S. Reiss, Wired Mag. **12.09** (2004).
[6] S. Hu and R. Wang, *Proceedings of the 2nd International Topical Meeting on High Temperature Reactor Technology, Beijing, China* (Institute for Nuclear and New Energy Technology, Beijing, China, 2004).
[7] http://www.pbmr.com
[8] http://web.mit.edu/pebble-bed
[9] J. Choi, A. Kudrolli, and M. Z. Bazant, J. Phys.: Condens. Matter **17**, S2533 (2005).
[10] J. Mullins, J. Appl. Phys. **43**, 665 (1972).
[11] R. M. Nedderman and U. Tüzün, Powder Technol. **22**, 243 (1979).
[12] R. M. Nedderman, *Statics and Kinematics of Granular Materials* (Cambridge University Press, Cambridge, UK, 1992).
[13] U. Tüzün and R. M. Nedderman, Powder Technol. **23**, 257 (1979).

[14] A. Medina, J. A. Cordova, E. Luna, and C. Trevino, Phys. Lett. A **220**, 111 (1998).
[15] A. Samadani, A. Pradhan, and A. Kudrolli, Phys. Rev. E **60**, 7203 (1999).
[16] J. Choi, A. Kudrolli, R. R. Rosales, and M. Z. Bazant, Phys. Rev. Lett. **92**, 174301 (2004).
[17] M. Z. Bazant, Mech. Mater. **38**, 717 (2006).
[18] C. H. Rycroft, M. Z. Bazant, G. S. Grest, and J. W. Landry Phys. Rev. E **73**, 051306 (2006).
[19] S. B. Savage, J. Fluid Mech. **92**, 53 (1979).
[20] J. T. Jenkins and S. B. Savage, J. Fluid Mech. **130**, 187 (1983).
[21] J. R. Prakash and K. K. Rao, J. Fluid Mech. **225**, 21 (1991).
[22] L. P. Kadanoff, Rev. Mod. Phys. **71**, 435 (1999).
[23] V. V. R. Natarajan, M. L. Hunt, and E. D. Taylor, J. Fluid Mech. **304**, 1 (1995).
[24] D. G. Schaeffer, J. Differ. Equations **66**, 19 (1987).
[25] E. B. Pitman and D. G. Schaeffer, Commun. Pure Appl. Math. **40**, 421 (1987).
[26] K. Kamrin and M. Z. Bazant (unpublished).
[27] A. Medina, J. Andrade, and C. Trevino, Phys. Lett. A **249**, 63 (1998).
[28] D. E. Mueth, G. F. Debregeas, G. S. Karczmar, P. J. Eng, S. R. Nagel, and H. M. Jaeger, Nature (London) **406**, 385 (2000).
[29] E. R. Weeks, J. C. Crocker, A. C. Levitt, A. Schofield, and D. A. Weitz, Science **287**, 627 (2000).
[30] J.-C. Tsai and J. P. Gollub, Phys. Rev. E **70**, 031303 (2004).
[31] M. Menon and D. J. Durian, Science **275**, 1920 (1997).
[32] J. S. Goodling, R. I. Vachon, W. S. Stelpflug, and S. J. Ying, Powder Technol. **35**, 23 (1983).
[33] A. J. Sederman, P. Alexander, and L. F. Gladden, Powder Technol. **117**, 255 (2001).
[34] Y. Cohen and A. B. Metzner, AIChE J. **27**, 705 (1981).
[35] D. Vortmeyer and J. Schuster, Chem. Eng. Sci. **38**, 1691 (1983).
[36] S. M. White and C. L. Tien, Waerme- Stoffuebertrag. **21**, 291 (1987).
[37] A. Kadak and M. Z. Bazant, *Proceedings of the 2nd International Topical Meeting on High Temperature Reactor Technology, Beijing, China* (Institute for Nuclear and New Energy Technology, Beijing, China, 2004).
[38] W. K. Terry, H. D. Gougar, and A. M. Ougouag, Ann. Nucl. Energy **29**, 1345 (2002).
[39] H. D. Gougar, W. K. Terry, and A. M. Ougouag, *Proceedings of the Conference on High-Temperature Reactors, Petten, NL* (International Atomic Energy Agency, Vienna, Austria, 2002).
[40] C. du Toit, *Proceedings of the Conference on High-Temperature Reactors, Petten, NL* (International Atomic Energy Agency, Vienna, Austria, 2002).
[41] A. M. Ouguag, J. J. Cogliati, and J.-L. Kloosterman, *Proceedings of the Topical Meeting on Mathematics and Computation, Avignon, France*, (American Nuclear Society, LaGrange Park, IL, 2005).
[42] L. E. Silbert, D. Ertaş, G. S. Grest, T. C. Halsey, D. Levine, and S. J. Plimpton, Phys. Rev. E **64**, 051302 (2001).
[43] J. W. Landry, G. S. Grest, L. E. Silbert, and S. J. Plimpton, Phys. Rev. E **67**, 041303 (2003).
[44] P. A. Cundall and O. D. L. Strack, Geotechnique **29**, 47 (1979).
[45] J. Litwiniszyn, Rheol. Acta **2/3**, 146 (1958).
[46] G. Y. Onoda and E. G. Liniger, Phys. Rev. Lett. **64**, 2727 (1990).
[47] C. S. O'Hern, S. A. Langer, A. J. Liu, and S. R. Nagel, Phys. Rev. Lett. **88**, 075507 (2002).
[48] S. Torquato, T. M. Truskett, and P. G. Debenedetti, Phys. Rev. Lett. **84**, 2064 (2000).
[49] M. Newey, J. Ozik, S. M. van der Meer, E. Ott, and W. Losert, Europhys. Lett. **66**, 205 (2004).
[50] Z. S. Khan, W. A. Tokaruk, and S. W. Morris, Europhys. Lett. **66**, 212 (2004).
[51] Z. S. Khan and S. W. Morris, Phys. Rev. Lett. **94**, 048002 (2005).
[52] T. Shinbrot and F. J. Muzzio, Phys. Rev. Lett. **81**, 4365 (1998).
[53] T. Shinbrot, Nature (London) **429**, 352 (2004).